Received: 27 June 2017 | Revised: 16 November 2017 | Accepted: 22 November 2017

DOI: 10.1002/pip.2979

WILEY PROGRESS IN PHOTOVOLTAICS

RESEARCH ARTICLE

The view-factor effect shaping of I-V characteristics

Assaf Peled | Joseph Appelbaum

School of Electrical Engineering, Tel-Aviv University, Tel-Aviv 69978, Israel

Correspondence
Assaf Peled, School of Electrical Engineering, Tel-Aviv University, Tel-Aviv 69978, Israel
Email: assafpeled@gmail.com

Abstract

The diffuse radiation collected by PV modules is coupled with a view-factor of the module to sky, which varies across the module surface in multiple-row installations. The view-factor variation inflicts current mismatch between the module strings by virtue of the nonuniform solar flux absorbed by the module's cells, leading in turn to an overall reduction in performance. The following study establishes a theoretical framework for predicting the step-wise properties of the module I-V curve following the current mismatch induced by the view-factor. To illustrate the steps pattern, synthetic I-V curves are derived by using the 5-parameter PV cell single-diode model in conjunction with 3 additional parameters that account for the cell's avalanche breakdown. We investigate the steps pattern as well as the power losses incurred by the view-factor by simulating different types of PV deployments over a range diffuse radiation rates. For a tilted module installed on a horizontal plane, for instance, the study predicts a reduction in power ranging 2.8% to 25%, depending on the precentage diffuse radiation on the site in question.

KEYWORDS

current mismatch, diffuse irradiation, I-V curve steps, view-factor to sky

1 | INTRODUCTION

The study of solar radiation impact on PV cells traditionally distingushes between 3 irradiation components, namely, the direct, diffuse, and reflected. While the direct fraction is determinstic in nature and rests on well-known equations, the diffuse fraction is subject to stochastic environmental factors. Generally speaking, the diffuse fraction absorbed by a PV module can be envisioned as arriving from multiple sources distributed across the sky-dome. Consequently, a *sky view-factor* parameter can be attributed to different parts on the module front (or back) surface, so as to account for the fact that these parts "see" uneven portions of the visible sky. Depending on the site of installation, the diffuse fraction often covers large proportions of the total radiation collected by the modules, such that any phenomenon within the PV modules ascribed to the diffuse irradiation becomes well pronounced.[1]

View-factors have wide range applications in radiative heat transfer. Numerical methods have been developed to calculate the view-factors by Monte-Carlo method,[2,3] Ray tracing method,[4] and others.[5,6] View-factor catalogues are published in the literature.[7-9] All the above references deal with thermal radiation between surfaces. In PV systems, the view-factor is connected to the diffuse radiation from sky (not considering the reflective radiation in the present study) reaching the collector; hence, the view-factor is defined between a collector and sky.

When calculating a PV array, string, or cell's conversion of diffuse radiation into electrical energy, one needs to couple the diffuse component with a view-factor value. The detrimental effects associated with the view-factor have been addressed in a series of recent works that established the view-factor as an emerging topic of technical significance. Appelbaum[10] formulated analytical expressions for the sky view-factor as function of the PV installation's geometrical parameters. The view-factor equations developed by Appelbaum later served Peled and Appelbaum[11] in estimating the power losses resulting from the view-factor effect in 2 case-study sites throughout a 2-year period. Peled and Appelbaum[11] proposed several alternative interconnection strategies to tackle the module's internal current mismatch brought about by the view-factor effect. Appelbaum and Aronescu[12] extended the view-factor theory to address rooftop installations in the presence of obscuring structures. A general mathematical expression for the view-factor to sky was developed in Maor and Appelbaum[13] for collectors mounted on sloped planes where the azimuths of the planes and the collectors do not coincide.

The view-factor has also been treated rather extensively in the context of bifacial PV arrays, where concise models were formulated to account for the radiative transfer of the array's surroundings onto

the bifacial modules backside. To do so, these models[14] presuppose an isotropic scattering from reflecting surfaces and formulate a numerical integration to compute the overall reflected radiation from nearby elements around the array. Hansen et al[15] elaborate on the proposed view-factor model and show remarkable empirical-to-theoretical fitting results for the irradiance of 6 outdoor rear-facing cells. A formulation of the view-factor of rear-side collectors with shaded and unshaded ground has equally been presented by Appelbaum[16] alongside the comprehensive treatment of the different models of the view-factor with respect to a variety of array configurations.

Bifacial PV panels deployed in multiple rows in a PV field in Appelbaum[17] compare the annual incident irradiation on collectors deployed vertically with the annual incident irradiation on collectors deployed with an optimal tilt angle. The present study discusses the view-factor to sky of the front facing modules.

For reader's convenience, we shall first reiterate the main equation governing the view-factor effect to lay the groundwork for the succeeding parts. A multiple-row PV installation is characterized by a number of parameters pertaining to the geometrical constellation of its modules. Each module consists of series-connected substrings, with each substring comprising similar number of cascaded cells.

In accordance with the model proposed by Appelbaum,[10] the individual module in multiple-row installation follows the geometrical conventions depicted in Figure 1, where each module is tilted β and the net distance between 2 succeeding rows is D. In addition, each module is segmented along its width H into discrete number of rectangular subareas, each of which corresponding to a single strip (row of cells). Thus, each such subarea is assigned a different view-factor, depending on the installation's geometrical features. The example in Figure 1 shows 6 strips layout where a distinct view-factor $F_1 - F_6$ is designated for each subarea.

Photovoltaic collectors are deployed in rows in a solar field, with the length of each row being much higher than its height, such that the collector may be regarded as having an infinite length. The calculation of the view-factors may be based on Appelbaum and Aronescu.[12] A more convenient approach is the "cross-string" rule by Hottel.[18] The underlying equation for the view-factors of the above 6 strips layout is where

$$F_i = \frac{H/N + \left[\left(D + \alpha_i \cdot H\cos\beta\right)^2 + \left(\gamma_i \cdot H\sin\beta\right)^2\right]^{1/2} - \left[\left(D + \omega_i \cdot H\cos\beta\right)^2 + \left(\psi_i \cdot H\sin\beta\right)^2\right]^{1/2}}{2H/N} \quad (1)$$

$$\{\alpha_i\}_{i=1}^{N} = \frac{N+1-i}{N}, \quad \{\gamma_i\}_{i=1}^{N} = \frac{i-1}{N}, \quad \{\omega_i\}_{i=1}^{N} = \frac{N-i}{N}, \quad \{\psi_i\}_{i=1}^{N} = \frac{i}{N},$$

and N denotes the number of cell rows in the module.

Setting $N = 6$, Figure 2 plots $F_1 - F_6$ against the tilt β when the distance between rows and the module width are set to D = 0.68m and H = 0.941m (Trina ALL-MAX), respectively. For the given value of H, D is the row-to-row distance for corresponding the shadow length when the solar path attains minimum elevation angle, namely, on December 21 at solar noon (latitude 32°N).

The vertical lines in Figure 2 are intersecting the view-factor curves on specific tilt angles between 20° and 50°. As expected, increasing the tilt angle entails an overall reduction of the view-factors, as the modules in successive rows obscure greater portions of the visible sky.

Moreover, increasing the module tilt correlates to the percentage difference between the top and bottom strips and in effect contributes to the imbalance between the strips currents. Taking β = 30°, D = 0.68m and H=0.941m for example, it is found that F_1 = 0.9258, F_2 = 0.9084, F_3 = 0.8850, F_4 = 0.8531, F_5 = 0.8095 and F_6 = 0.7507. The top-bottom percentage difference

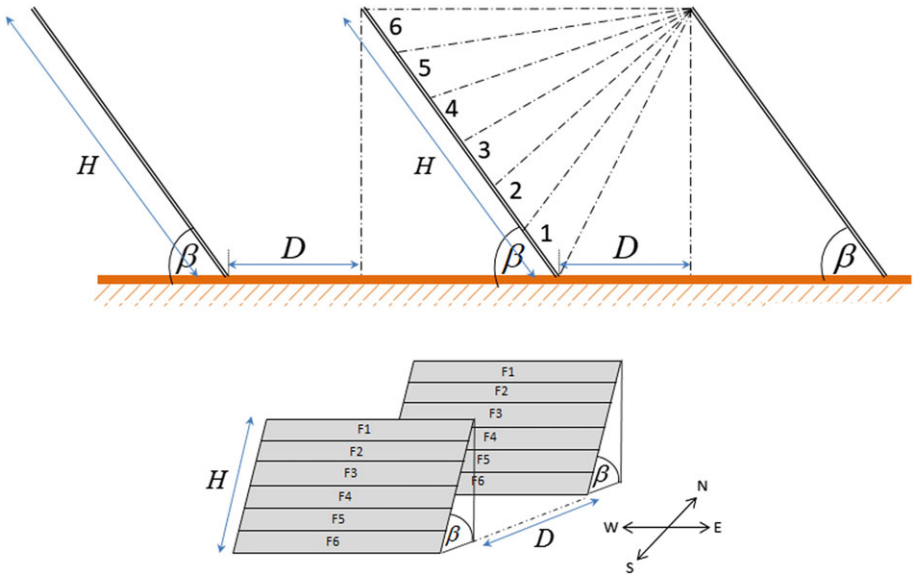

FIGURE 1 Top, Typical installations of PV modules divided into 6 substrings. Bottom, Illustrative diagram for calculating the sky view-factors [Colour figure can be viewed at wileyonlinelibrary.com]

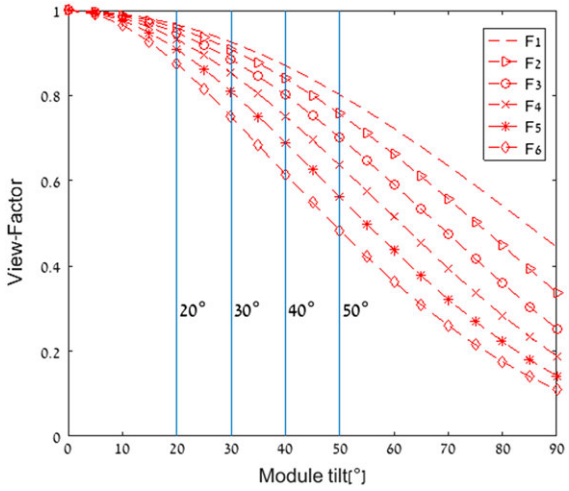

FIGURE 2 Variation of 6 view-factor values pertaining to Figure 1 with the tilt angle, when D = 0.68 m, H = 0.941 m [Colour figure can be viewed at wileyonlinelibrary.com]

$\Delta F^{\%}_{1-6} = 100(F_1 - F_6)/F_1$ rises from 9.46% when β = 20° up to 39.77% when β = 50°.

1.1 | Aim of study and method

With the principles of the view-factor effect in mind, we set about to explore how this effect can manifest itself within the PV module I-V characteristic. In a typical silicon-crystalline module, the cells are all connected in series and arranged in substrings. The multiple connections between the cells are augmented by the use of bypass diodes, allowing series substrings to function in the presence of various failures. Each substring is typically bridged by a parallel bypass diode that protects the substrings cells and is connected in an opposite polarity. Under normal operation, substrings are forward biased and the bypass diodes are inactive. If a substring becomes reverse biased due to an internal mismatch between its cells, then the bypass diode activates to circumvent the mismatched cells or substrings from dissipating power. When that happens, the operating point of that particular cell or substring's I-V curve is shifted to the respective substring's reverse bias region.

The said current mismatch between substrings can be brought about by a variety of failures[19] related to degradation,[20] overheating,[21] manufacturing defects, or nonuniform soiling.[22] A comprehensive study has also been dedicated to the decrease in PV performance due to partial shading.[23-28] Of this partial list of failure modes, system's power loss due to partial shading has the closest conceptual relevance to our study, as the current mismatch that is caused by the shading together with the incorporation of bypass diodes manifests itself in the formation of steps across the module I-V curve.

In the following study, however, we argue that the said step patterns are not merely a product of shading losses, but can be equally brought about by the presence of nonuniform irradiance, resulting from the view-factor effect. As we shall demonstrate, the lack of consistency between the substrings with respect to their irradiance induces imbalanced photo-generated currents in them. Consequently, the module I-V characteristic departs from its normal shape and instead exhibits steps whose position corresponds to points where the bypass diode are activated. To show this, we simulate a series of synthetic module I-V curves and apply the above theory to modulate these curves and estimate the implications on the PV module performance stemming from the view-factor effect.

It should be noted that the analysis hereby applies for the sake of simplicity to an isotropic sky diffuse model, such that the diffuse irradiance impinging the modules is uniformly distributed across them irrespective of the angle of incidence. We also regard any portion of diffuse radiation as a whole, by disregarding its spectral constituents that may or may not affect the cells. Taking these effects into account calls for an in-depth study, currently left for future work. Rather, the underlying premise of the following study is that analyzing the module performance in the presence of the view-factor effect should provide a valuable overview of the view-factor elements that adversely affect the PV modules performance.

The single-diode model for a PV cell follows the well-known 5-parameter I-V equation in the positive voltage range:

$$I(V) = I_{ph} - I_0\left(\exp\left(\frac{V + I\cdot R_s}{nV_t}\right) - 1\right) - \frac{V + I\cdot R_s}{R_{sh}} \tag{2}$$

with I_{ph}, I_0, R_s, R_{sh}, n, V_t being the photo-generated current, reverse-saturation current, series resistance, shunt resistance, diode ideality-factor, and thermal voltage, respectively. Bishop[29] augmented Equation 2 with 3 additional parameters that account for the cell behavior in the negative region:

$$I(V) = I_{ph} - I_0\left(\exp\left(\frac{V + I\cdot R_s}{nV_t}\right) - 1\right) - \frac{V + I\cdot R_s}{R_{sh}} - \alpha\frac{V + I\cdot R_s}{R_{sh}}\left(1 - \frac{V + I\cdot R_s}{V_{br}}\right)^{-m} \tag{3}$$

where V_{br} is the junction breakdown voltage, α the fraction of Ohmic current involved in avalanche breakdown, and m the avalanche breakdown exponent. Note that the additional term in Equation 3 vanishes for α = 0 and the cell's I-V curve retains its original form irrespective of the breakdown mechanism. Shown in Figure 3 is the extended model, with the additional avalanche breakdown term denoted by the current source I_{br}.

We use the Trina-Solar ALL-MAX 260W as our reference module, featuring 60 series-connected cells and front surface dimensions of 1650 × 992 mm. The LMA fitting algorithm[30] is then served to extract the single solar cell parameters in Equation 3 with a nominal irradiance 1000 W/m^2. V_{br} = − 15 V is set to be the cell's breakdown voltage. The α and m parameters are adjusted iteratively[31] on the basis

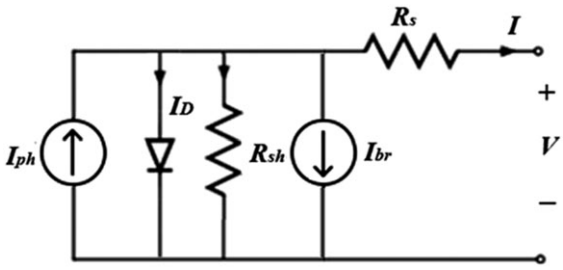

FIGURE 3 PV cell equivalent circuit

of the results of the remaining parameters, namely, I_{ph}, I_0, R_s, R_{sh} and n, as follows:

$$\alpha = R_s/(R_{sh}-R_s)-R_{sh}I_0/(n\cdot V_T) \tag{4}$$

$$m = \left| \frac{\ln\left\{\frac{R_{sh}}{\alpha(V+I\cdot R_s)}\left[I_{ph}-I_0\left(e^{(V+I\cdot R_s)/V_T n}-1\right)-\frac{V+I\cdot R_s}{R_{sh}}-I\right]\right\}}{\ln\left[1-\frac{V+I\cdot R_s}{V_{br}}\right]} \right| \tag{5}$$

The substring electrical parameters (denoted by superscript "s") can be derived from those of a single cell (denoted by superscript "c") by a set of simple operations:

$$I^s_{ph} = I^c_{ph},\ \ I^s_0 = I^c_0\ ,\ \ n^s = S\cdot n^c,\ \ R^s_s = S\cdot R^c_s,\ \ R^s_{sh} = S\cdot R^c_{sh} \tag{6}$$

where S denotes the number of series-connected cells in a substring. The reference cell's electrical parameters retrieved via fitting are tabulated in Table 1 for 3 representing global irradiation at nominal levels (according to manufacturer's data sheet) of 1000, 600, and 400 W/m^2. We use the latter gradually decreasing nominal values as a reference point for the succeeding results, to account for real-life scenarios in which the global irradiation diminishes as the diffuse irradiation increases in magnitude.

Our model proposes to modulate the STC I-V curve as synthesized by the parameters in Table 1, by introducing changes into the cell's photocurrent I_{ph}, resulting directly from the view-factor effect. Neglecting the reflected irradiation component, the global irradiation impinging on a solar cell is a linear function of the direct beam irradiance (G_b), the diffuse irradiance (G_d), and the sky view-factor (F_{sky}):

$$G = G_b + F_{sky}\cdot G_d \tag{7}$$

Denoting G_0 as the nominal irradiation, the module photocurrent is proportional to the global irradiance:

$$I_{ph}(G) = I_{ph}(G_0)\cdot G/G_0 \tag{8}$$

Substituting Equation 7 into Equation 8, we get

$$I_{ph}(G) = I_{ph}(G_0)\cdot\left(G_b + F_{sky}\cdot G_d\right)/G_0 \tag{9}$$

Moreover, previous studies that rest on empirical data[32,33] concluded that the shunt resistance follows an exponential model that exhibits an inverse behavior with respect to the global irradiance:

$$R_{sh} = R_{sh,ref} + \left(R_{sh,0}-R_{sh,ref}\right)\cdot\exp(-5.5G/G_0) \tag{10}$$

where $R_{sh,\ ref}$ denotes the shunt resistance obtained through fitting (Table 1). For Si-crystalline cells, the exponential model in Equation 10 assumes $R_{sh,\ 0} = 4R_{sh,\ ref}$. Our analysis assumes that apart from the photocurrent and the shunt resistance, the remaining parameters in Equation 3 are to a large extent independent of the irradiance. In an ideal case, the irradiance is uniformly distributed across the 60 cells comprising the module, by virtue of identical view-factor values that are associated with each cell. In practice, however, F_{sky} gradually drops starting from the module top strip downwards, inducing current mismatch between substrings. Figure 4 illustrates the view-factor distribution among the 60 cells when the module is either vertically or horizontally oriented. Note that the module comprises 3 substrings altogether, each of which has 20 series-connected cells (in a typical silicon-crystalline module) protected by a single diode. Judging from Figure 4, we may expect the module orientation to be an instrumental parameter in shaping the module I-V curve.

2 | RESULTS AND DISCUSSION

Figure 5 plots the I-V and P-V curves of the reference module at 1000 W/m^2 following the fitting method described above and

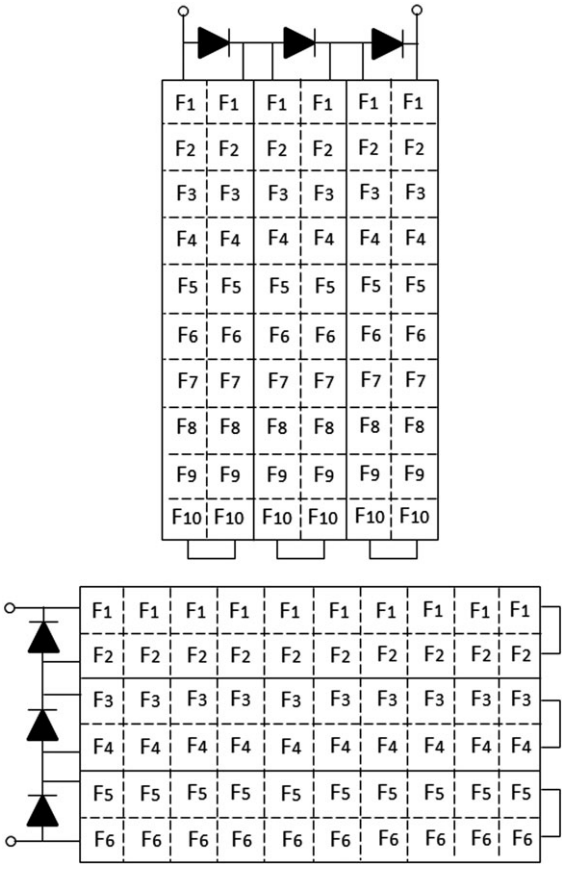

FIGURE 4 Top, View-factor distribution across a vertically oriented module. Bottom, View-factor distribution across a horizontally oriented module

TABLE 1 Reference cell parameters

Nominal Irradiation, W/m^2	R_s, mΩ	R_{sh}, Ω	n	I_0, nA	I_{ph}, A	α	m
1000	5.6	41.86	1.07	0.866	9.006	$2.095\cdot10^{-5}$	2
600	5.6	46.49	1.025	0.897	5.413	$3.042\cdot10^{-5}$	2.004
400	5.6	55.77	0.972	0.818	1.804	$5.585\cdot10^{-5}$	2.002

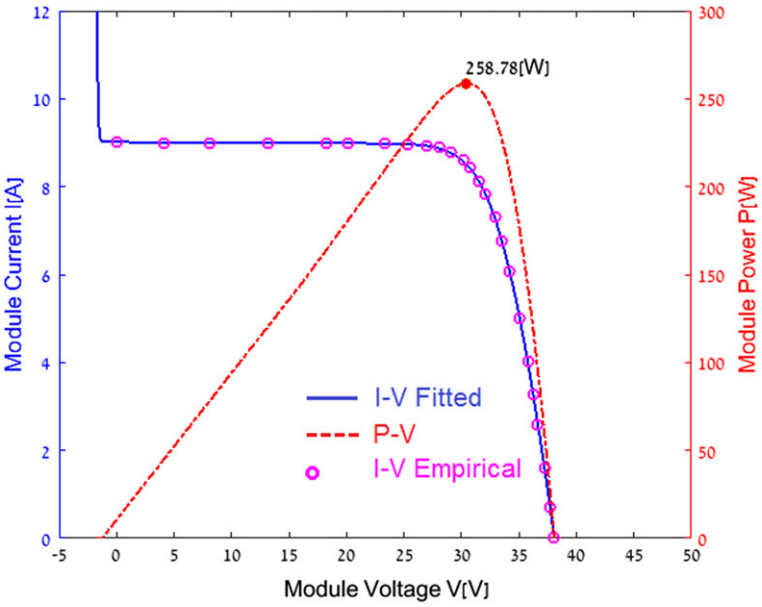

FIGURE 5 Trina ALL-MAX reference module fitted and theoretical I-V curves and P-V curve at 1000 W/m^2 [Colour figure can be viewed at wileyonlinelibrary.com]

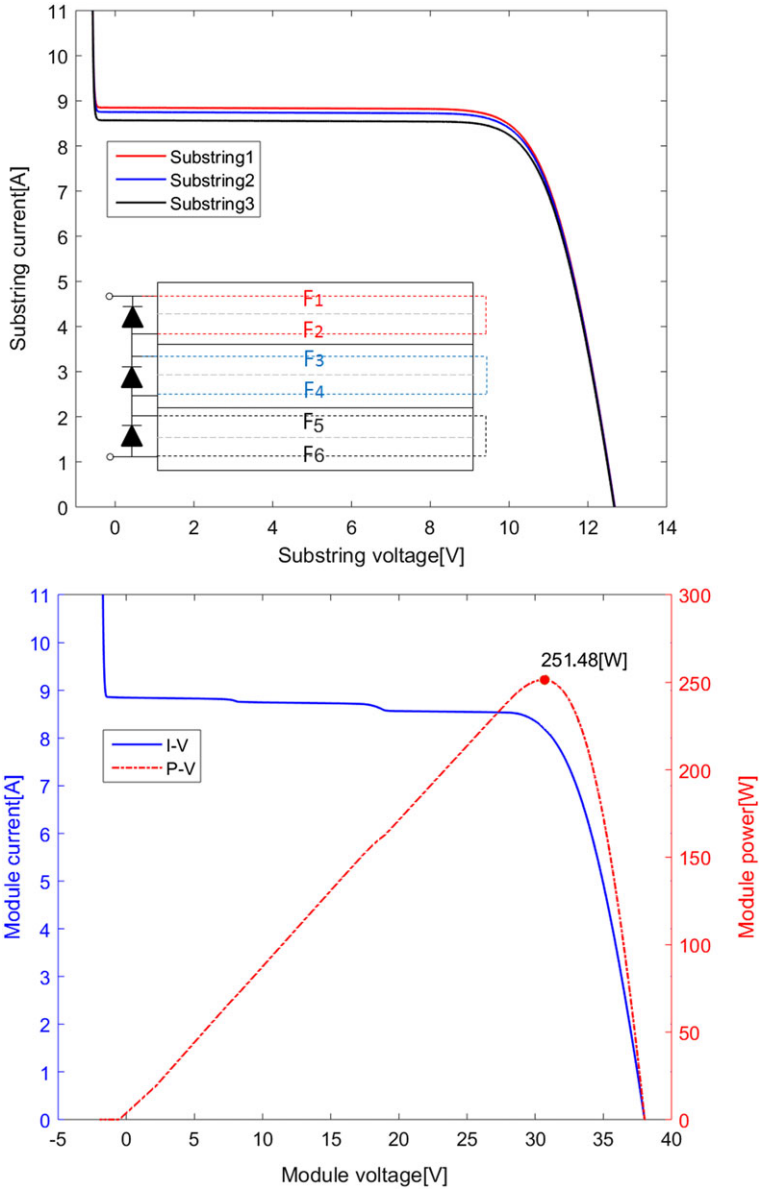

FIGURE 6 Top, I-V of 3 substrings of Trina ALL-MAX module, horizontally oriented, tilted 30° with 20% diffuse irradiation w.r.t. a nominal G_0 = 1000 W/m^2. Bottom, Resulting I-V and P-V curves [Colour figure can be viewed at wileyonlinelibrary.com]

corresponds to an ideal case where unity view-factor is assigned to all 60 cells. The I-V curve rises sharply around −0.6 V, at which point all 3 bypass diodes (Figure 4) are activated. We assume that the bypass diode follows the ideal diode equation:

$$I(V) = I_r(\exp(qV/KT)-1) \quad (11)$$

where I_r is the diode reverse current, set to a typical value of 0.1 nA. The theoretical I-V curve at 1000 W/m^2 is superimposed by Trina ALL-MAX empirical samples. The maximum-power is specified on the P-V curve, amounting to 258.8 W_p. Satisfying fitting results were equally obtained for Trina's nominal I-V curves at 800, 600, 400, and 200 W/m^2, yielding nominal maximum-power points of 209.2, 158.3, 105.4, and 51.9 W_p, respectively. The incorporation of the view-factor effect from this point on would adversely affect the module power generation and divert the curve from its original outline.

In the nonideal case, the view-factor is introduced into the I-V computations, and the individual substrings I-V characteristics become nonidentical because of their imbalanced photocurrents I_{ph}. When the module is oriented horizontally, Figure 4 theorizes 6 view-factors, each assigned to one strip of series cells. The 6 view-factors are calculated by Equation 1, setting the number of cell strips to N = 6. Each pair of successive strips comprises one substring, which then connects in parallel to a bypass diode. Since each one of the 3 substrings effectively acquires a unique photocurrent, we expect to observe the discrepancy between them in the form of 3 steps across the module's I-V positive region. However, when the module is oriented vertically, 10 different view-factors synthesize an individual substring, such that the steps—prior to connecting the bypass diode—are all found deep into the substring's negative region. Connecting a bypass diode to the substring essentially eliminates the said negative region all the way up to −0.6V, where the diode is activated. Moreover, since these 10 view-factors are common to all 3 substrings, the photocurrents of these substrings will be equal, resulting in the module I-V having no steps in the positive region. Thus, the mere act of orienting a module vertically removes step patterns from the module I-V characteristics.

We consider first a multiple-row deployment in which the individual Trina ALL-MAX module in Figure 5 (at 1000 W/m^2) is exposed to 20% diffuse (hence, 80% direct beam) irradiance and tilted at β = 30°. The distance between 2 successive rows stands on D = 0.68 m, corresponding to the horizontally oriented modules. Figure 6 (top) plots the 3 substrings curves according to their order in the module, top to bottom. Note that although each of the 3 substrings' I-V curve covers 2 view-factors, the steps induced by the 2 view-factors lie well into the negative region and are eliminated, in effect, by the inclusion of the bypass diode. Every substring I-V curve therefore exhibits smoothness. When the 3 substrings are cascaded to form the module, the variation in their photocurrents gives rise to steps in the positive region. Figure 6 (bottom) plots the resulting I-V and P-V curves in which the steps and notches are seen, respectively, where the steps height corresponds to the gap between the substrings I-V's. The power losses with respect to the STC module amount to 2.82%.

In Figure 7, the formation of steps and notches is slightly more observable by the increase of percentage diffuse irradiance from 20% to 50%, attributed to a nominal irradiation of 600 W and peak

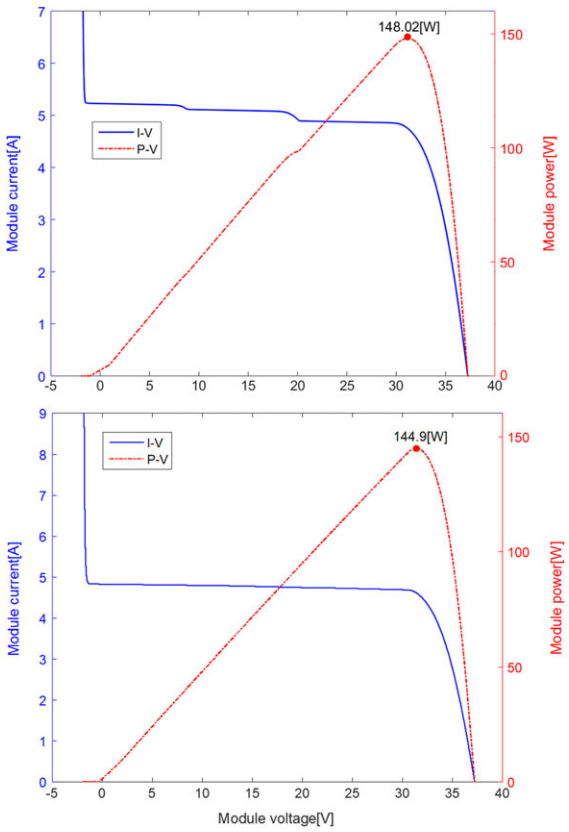

FIGURE 7 Top, Trina ALL-MAX module I-V and P-V, horizontally oriented and tilted 30° with 50% diffuse irradiance w.r.t. a nominal G_0 = 600 W/m^2. Bottom, I-V and P-V, vertically oriented, tilted 30° with 50% diffuse irradiance w.r.t. a nominal G_0 = 600 W/m^2 [Colour figure can be viewed at wileyonlinelibrary.com]

power of 158.31 W. The top inset shows the horizontally oriented module I-V and P-V curves at β = 30°, D = 0.68 m, 50% diffuse irradiance, while the bottom inset shows the vertically oriented module at β = 30°, D = 1.2 m. The 10 view-factors calculated for the vertical module range from 0.93 on the top strip of cells down to 0.74 on the bottom strip of cells. Just as predicted, the vertical oriented module exhibits no steps across its I-V curve because of the symmetry between the substrings' curves that renders the substrings photocurrent equal. The inclusion of steps hardly modifies the output power in these 2 cases, which is kept somewhat around 144 to 148 W, namely, a power loss of about 6.5% with respect to the nominal peak power of the module at 600 W/m^2. Similar analysis is given in Figure 8 when the percentage diffuse irradiance is 70% at a nominal global irradiation of 400 W/m^2

Figures 6--8 invite a broader examination of the vertical and horizontal modules output power across a wider range of percentage diffuse irradiance values. Figure 9 plots the horizontal and vertical module output power versus a steadily growing rate of diffuse irradiation, starting from 20%. The module in both cases is inclined at β = 30° and the distance between rows corresponds to the orientation, namely, D = 0.68 m and D = 1.2 m for the horizontal and vertical case, respectively. As expected, the output power decreases as the diffuse irradiance associated with the view-factor effect gradually overpowers the direct irradiance component. Moreover, the results validate our assumption that the presence of steps in the I-V characteristics has

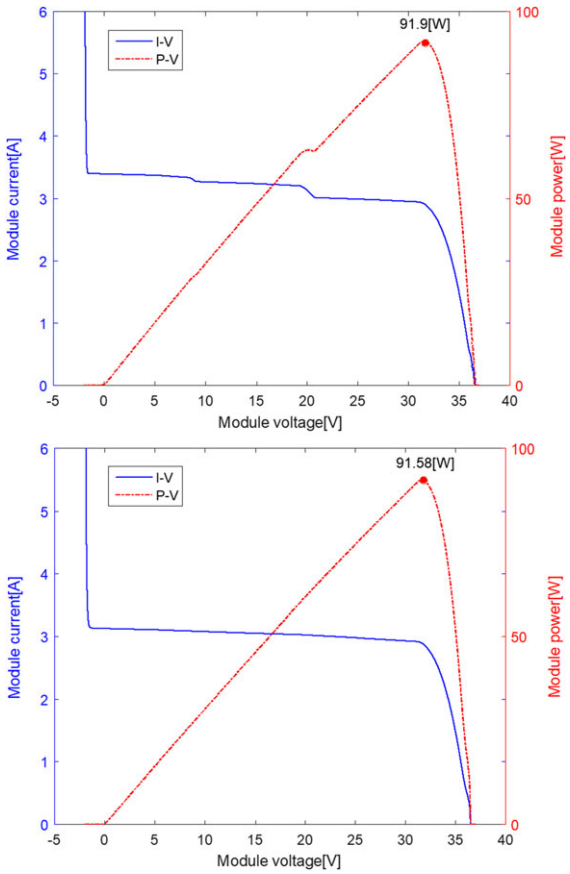

FIGURE 8 Top, Trina ALL-MAX module I-V and P-V, horizontally oriented and tilted 30° with 70% diffuse irradiance w.r.t. a nominal G_0 = 400 W/m^2. Bottom, I-V and P-V, vertically oriented, tilted 30° with 70% diffuse irradiance w.r.t. a nominal G_0 = 400 W/m^2 [Colour figure can be viewed at wileyonlinelibrary.com]

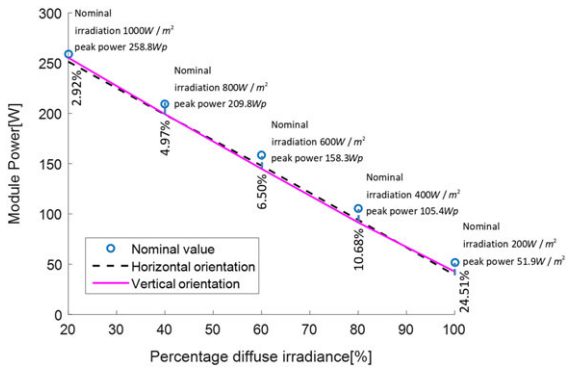

FIGURE 9 The output power of Trina ALL-MAX horizontally and vertically oriented modules vs percentage diffuse irradiance. The modules are tilted 30°. Selected points along the graph are annotated with their designated nominal irradiation and peak power. The percentage power loss expected at each point is annotated vertically [Colour figure can be viewed at wileyonlinelibrary.com]

little or no correlation with the module peak power. A selection of points on Figure 9 is annotated with their attributed nominal irradiation and peak power, along with the percentage power loss expected at each point. This loss ranges 2.8%, pertaining to clear-sky state, up to about 25% in the extreme case where the diffuse irradiance dominates the irradiation profile.

Since the view-factor effect on the module performance is nonlinear, we may also calculate an analytical approximation for the output power as function of the percentage diffuse radiation. A polynomial fitting of the curves shown in Figure 9, normalized by P_{max} = 258.78 W of the module at a nominal 1000 W/m^2, reveals that the power for β = 30° behaves as follows:

$$P_h(d)/P_{max} = 1 - 0.0082d - 4.4731\times10^{-6}d^2 \quad (12)$$

$$P_v(d)/P_{max} = 1 - 0.0095d - 8.759\times10^{-6}d^2 \quad (13)$$

where d denotes the percentage diffuse irradiance and $P_h(d)$, $P_v(d)$ the output power of the horizontal and vertical oriented modules, respectively. For a given width H of the PV module, either $P_h(d)$ or $P_v(d)$ is commensurate with the row-to-row distance D. On the basis of Figure 2 and Appelbaum,[10] decreasing the inclination angle β would also minimize the view-factor effect.

3 | CONCLUSIONS

Our study outlines a model for evaluating the extent to which steps are induced on a PV module I-V curve as a direct result of the view-factor variations across the module's surface. We first provide the equations that govern the view-factor's manipulation of the module performance. The model confirms that the reduction in performance of the PV module as inflicted by the view-factor effect is 2-fold: the formation of step patterns on one hand and the overall reduction in the output power on the other. We have shown that the distribution of view-factors throughout the module's front surface manifests itself differently when the module is oriented horizontally or vertically. While the model predicts the manifestation of steps in the horizontally oriented module in the positive range, as induced by the view-factor effect, the vertically oriented module contains no steps. More interesting is the fact that the output peak power following the view-factor effect is shown to be independent of the module orientation throughout the entire range of percentage diffuse irradiance. In either orientation, the analysis predicts an overall percentage power loss that ranges 2.8% up to about 25%, depending on the module inclination angle, the distance between the collector rows and the percentage diffuse irradiance. The study highlights the view-factor's coupling with the diffuse irradiation as an additional factor in forming steps across the I-V characteristic—a phenomenon typically ascribed to PV systems' shaded conditions that are inflicted by the direct beam radiation.

ORCID

Assaf Peled http://orcid.org/0000-0001-6502-3017

REFERENCES

1. Kadar P. The effect of the diffuse irradiation on the PV plants' producion. 2016. IEEE 14th international symposium on applied machine intelligence and informatics. *Slovakia*.
2. Mirhosseini M, Saboonchi A. Monte Carlo method for calculating local factor for the practical case in material processing. *Int Commun Heat Mass Transfer*. 2011;38(8):1142-1147.

3. Vujicic MR, Lavery NP, Brown SGR. View factor calculation using the Monte Carlo method and numerical sensitivity. *Commun Numer Methods Eng*. 2006;22:197-203.
4. Walker T., Xue S.C., Barton G.W., Numeical determination of radiative view factors using ray tracing. *J Heat Transfer*, 2010. 132:072702-1:072720-6, 7, 072702.
5. Bopche SB, Sridharan A. Determination of view-factors by contour integral technique. *Ann of Nuclear Energy*. 2009;36(11-12):1681-1688.
6. Yoo SH. Einstrahlzahlen fuer die Strahlungsaustausch-Berechnung in schiefwinkligen Raeumem. *Gesund Ing*. 1994;115:252-256.
7. Howell JR. *A Catalogue of Radiation Configuration Factors*. New- York: McGraw Hill; 1982.
8. Walton G.N., Calculation of obstructed view-factors by adaptive integration. NISTIR 6925, 2002.
9. Martinez I., *Radiative View Factors*, 1995-2015.
10. Appelbaum J. Current mismatch in PV panels resulting from different locations of cells in the panel. *Solar Energy*. 2016;126:264-275.
11. Peled A., Appelbaum J., Enhancing the power output of PV modules by considering the view factor to sky effect and rearranging the interconnections of solar cells. *Progress in Photovoltaics:Research and Applications* 2017; DOI: https://doi.org/10.1002/pip.2896.
12. Appelbaum J, Aronescu A. View factors of photovoltaic collectors on roof tops. *Renewable and Sustainable Energy*. 2016;8(2):025302
13. Maor T, Appelbaum J. View-factor of photovoltaic collector systems. *Journal Solar Energy*. 2012;80:78-88.
14. *Sandia National Laboratories:* view-factor models for bifacial PV-performance, via https://pvpmc.sandia.gov/pv-research/bifacial-pv-project/bifacial-pv-performance-models/ray-tracing-models-for-backside-irradiance/view-factor-models/
15. Hansen CW, Gooding RL, Guay N, et al. A detailed model of rear-side irradiance for bifacial PV modules. *Proceedings of 2017 IEEE Photovoltaics Specialists Conference*, Washington, DC. June 2017.
16. Appelbaum J. The role of view factors in solar photovoltaics fields. *Renew Sustain Energy Rev*. 2018;81:161-171.
17. Appelbaum J. Bifacial photovoltaic panels field. *Renew Energy*. 2016;85:338-343. https://doi.org/10.1016/j.renene.2015.06.050
18. Hottel HC, Sarofin AF. *Radiative Transfer*. New-York: McGraw-Hill; 1967:31-39.
19. Jordan DC, Silverman TJ, Wohlgemuth JH, et al. Photovoltaic failure and degradation modes. *Progr Photovolt: Res Appl*. 2017;25(4):318-326.
20. Jordan DC, Kurtz SR. Photovoltaic degradation rates—an analytical review, 2013. *Progr Photovolt: Res Appl*. 2013;21:1
21. Singh P, Ravindra NM. Temperature dependence of solar cell performance—an analysis. *Sol Energy Mater Sol Cells*. 2012;101:36-45.
22. Gostein M., Duster T., Thuman C., Accurately measuring PV soiling losses with soiling station employing power measurements. Proc. of 2015 IEEE 42nd Photovoltaic Specialist Conference (PVSC), 2015. DOI: https://doi.org/10.1109/PVSC.2015.7355993.
23. Quaschning V, Hanitsch R. Numerical simulation of current-voltage characteristics of photovoltaic systems with shaded solar cells. *Solar Energy*. 1996;56:6
24. Kawamura H, Kazuhito N, Yonekura N, et al. Simulation of I-V characteristics of PV module with shaded PV cells. *Solar Energy Materials & Solar Cells*. 2003;75(3-4):613-621.
25. Patel H, Agarwal V. Matlab-based modeling to study the effects of partial shading on PV Array characteristics. *IEEE Trans Energy Convers*. 2008;23:1
26. Sharma AK, Dwivedi R, Srivastava SK, Pathak CM. Performance analysis of a modified solar array under shadow conditions. *Renew Energy*. 1994;4(2):257-260.
27. Maki A, Valkealahti S, Leppaaho J. Operation of series-connected silicon-based photovoltaic modules under partial shading conditions. *Prog Photovolt Res Appl*. 2012;20(3):298-309.
28. Ziar H., Mansourpour S.,Afjey E., Kazemi M, Bypass diode characteristics effect on the behavior of solar PV array shadow condition, 2012, Power Electronics and Drive System Technology (PEDSTC) 229–233.
29. Bishop JW. Computer simulation of the effects of electrical mismatches in photovoltaic cell interconnection circuits. *Solar Cells*. 1988;25(1):73-89.
30. Appelbaum J, Peled A. Parameter extraction of solar cells—a comparative examination of three methods. *Sol Energy Mater Sol Cells*. 2014;122:164-173.
31. Ben-Or A, Appelbaum J. Performance analysis of concentrator photovoltaic dense-arrays under non-uniform irradiance. *Sol Energy Mater Sol Cells*. 2013;117:110-119.
32. Ruschel CS, Gasparin FP, Costa ER, Krenzinger A. Assessment of PV modules shunt resistance dependence on solar irradiance. *Solar Energy*. 2016;133:35-43.
33. De Soto W, Klein SA, Beckman WA. Improvement and validation of a model for photovoltaic array performance. *Solar Energy*. 2016;80:78-88.

How to cite this article: Peled A, Appelbaum J. The view-factor effect shaping of I-V characteristics. *Prog Photovolt Res Appl*. 2017;1–8. https://doi.org/10.1002/pip.2979